SACLANTCEN REPORT
serial no: SR- 344

SACLANT UNDERSEA RESEARCH CENTRE REPORT

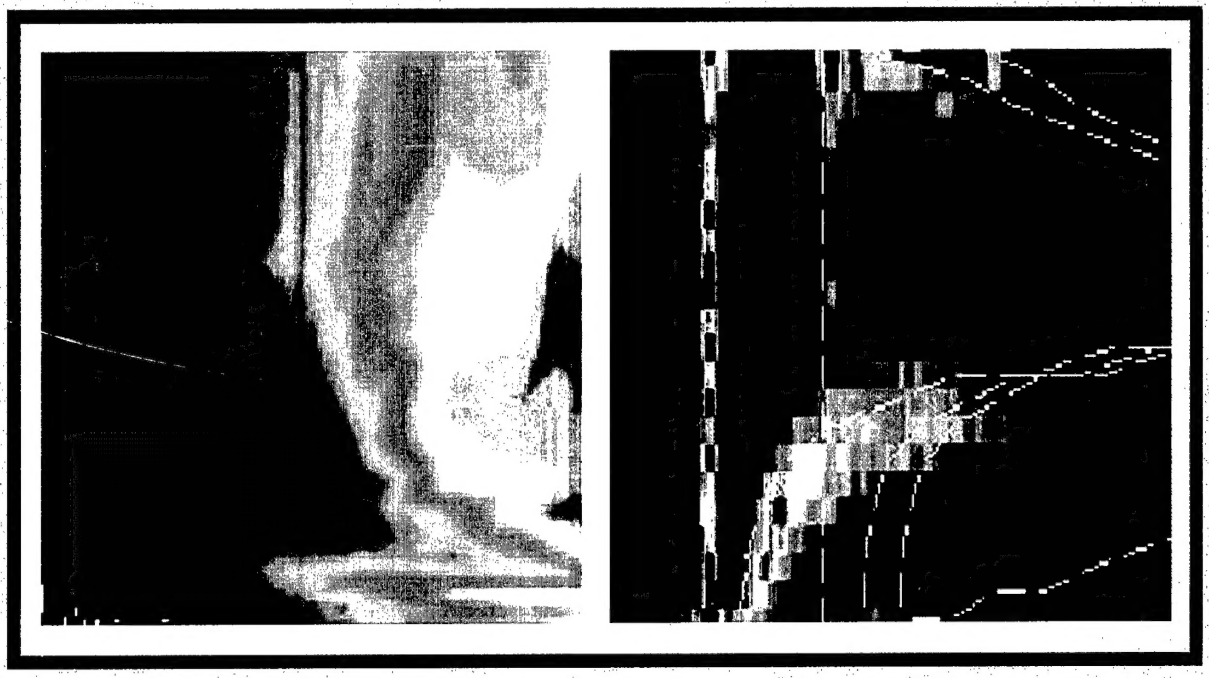

NORTH ATLANTIC TREATY ORGANIZATION ORGANISATION DU TRAITE DE L'ATLANTIQUE NORD

SACLANTCEN SR-344

Shallow water coupled scattering and reflection measurements

Charles W. Holland

The content of this document pertains to work performed under Project 04-C of the SACLANTCEN Programme of Work. The document has been approved for release by The Director, SACLANTCEN.

Jan L. Spoelstra
Director

intentionally blank page

Shallow Water Coupled Scattering and Reflection measurements

Charles W. Holland

Executive Summary: Sonar performance predictions for active systems operating in littoral regions require information on seabed reflection and scattering. Current NATO databases are often inadequate for supplying this information, especially in shallow water. Typically, survey measurements of these two parameters are conducted, processed, and analyzed in a completely separate way. In this report, we propose and demonstrate significant advantages to conducting reflection and scattering measurements in a coupled fashion. The coupling of the two analyses provides substantially more information on key seabed parameters.

The coupled approach is demonstrated by reflection and scattering data sets collected on the Malta Plateau. The results show that from 1- 6 kHz, the scattering and reflection are both dominated not by the water-sediment interface, but by sub-bottom layering. At one of the sites, the scattering at 3600 Hz was coming from surprisingly deep in the sediment (~10 meters sub-bottom) which indicates the need for next-generation databases to include such structures. The scattering strength increases with increasing frequency, indicating that sonar performance on the Malta Plateau may be optimal at lower frequencies.

intentionally blank page

Shallow Water Coupled Scattering and Reflection measurements

Charles W. Holland

Abstract: The characteristics of shallow water reverberation are often controlled by interaction with the seabed. This interaction includes both reflection and scattering processes. New techniques for measuring shallow water reflection and scattering have been developed that are coupled. The coupled nature of the measurements implies not only that they are conducted at the same locations, but that the measurements of the reflection provide significant keys for unravelling the scattering data. In particular, very high resolution geoacoustic data are extracted from the reflection data, which provide crucial inputs for the modelling of the scattering data. 1-6 kHz reflection and scattering measurements from the Malta Plateau illustrate the advantages of the coupled measurement approach.

Keywords:

Contents

1

Background and objectives

Over the past decades, a variety of physics-based seabed scattering models have been developed (e.g., Ivakin, 1986; Hines, 1990; Tang and Frisk, 1992, Mourad and Jackson, 1996; Yamamoto, 1996; Holland and Neumann, 1998, LePage and Schmidt, 2000). These models require increasingly detailed geoacoustic properties of the seabed. For example, the incident field on the sub-bottom volume or interfaces can be predicted only if the deterministic background properties of the sediment column are known. However, these properties are often unknown.

While core and other data can provide information on the very near sediment interface, sediment gradients are difficult to predict, and layering structure is generally unobtainable. Thus, often in the analysis of the scattering data, many of the deterministic geoacoustic properties (e.g., mean sound speed density, and attenuation) are "extracted" along with the statistical properties. The problem with this approach is that scattering data alone is generally inadequate to resolve each parameter unambiguously.

In an ideal experiment, each of the parameters required by the scattering model would be obtained independently. While this is difficult in practice, Holland and Neumann (1998) proposed and demonstrated in a deep-water environment that some of the key geoacoustic properties could be independently determined by geoacoustic inversion of seabed reflection measurements.

Following that approach, coupled measurements of seabed reflection and scattering have been made at shallow water sites on the Malta Plateau (see Fig. 1). By coupled, it is meant that the measurements are not only co-located, but sample commensurate spatial scales of the seabed. It is also meant that the processing and analyses employ commensurate assumptions and modelling. Finally, the analyses provide mutually beneficial information about the seabed and sub-bottom structure.

The coupled nature of the measurements and analysis with the Malta Plateau data illuminates several physical processes: 1) on the Malta Plateau the scattering arises principally from sub-bottom layers, rather than the water-sediment interface and 2) distinctness in the scattering strength from the various sites may be largely due to geometrical factors (i.e. layer thickness) rather than spatial variability in the scattering properties of the sediment.

The report is organized in the following way, first, the experiment locations and general environment of the Malta Plateau are described. Then the reflection measurements are discussed, highlighting the parameters that can be extracted from these data that are crucial for understanding (modelling) the scattering. Scattering measurements are then described and model-to-data predictions are provided which demonstrate the advantages

of the coupled approach. Conclusions on the data and methods are provided in the final section.

2
Environmental data

The bathymetry of experiment area is shown in Fig. 1. The area can be divided into two physiographic regions: the Ragusa Ridge, a lineated rocky outcrop forming a spine between Sicily and Malta (roughly defined by depths shallower than ~110 m) and the Malta Plateau. The latter is defined as that flat-lying area west of the Ragusa Ridge. Nearly the entire area of the Malta Plateau is covered with a high-porosity silty-clay sediment, although a few areas in the northern region (e.g., near Site 6) exhibit rock outcrops. In this report, reflection and scattering data sites on the Malta Plateau (Sites 1, 4 and 10) will be discussed.

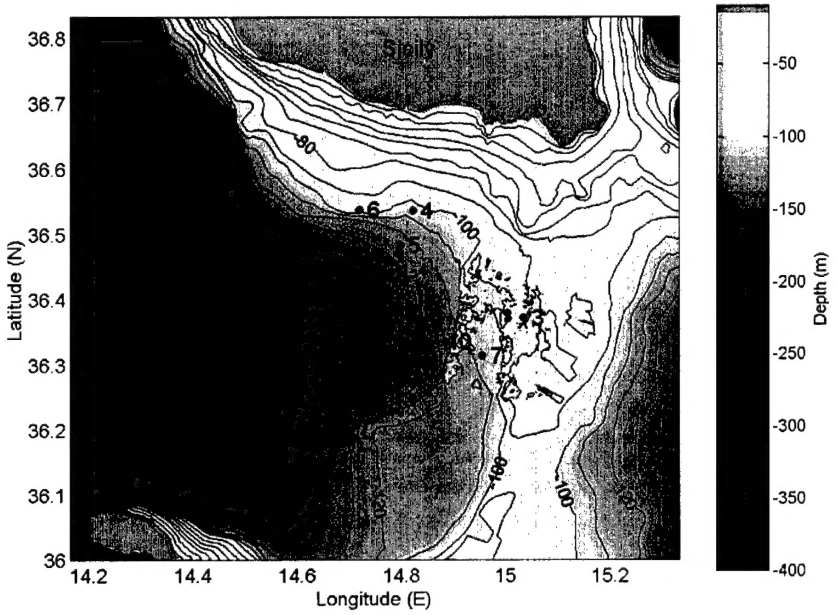

Figure 1 *Bathymetry in metres and site locations (in white) on the Malta Plateau and Ragusa Ridge.*

Seismic reflection data from Site 4 to Site 1 is shown in Fig. 2. Note that the seafloor is very smooth and flat, with slopes of the water-sediment interface and sub-bottom horizons much less than 1°. At Site 4, the first sediment layer is about 10 m thick and thins seaward.

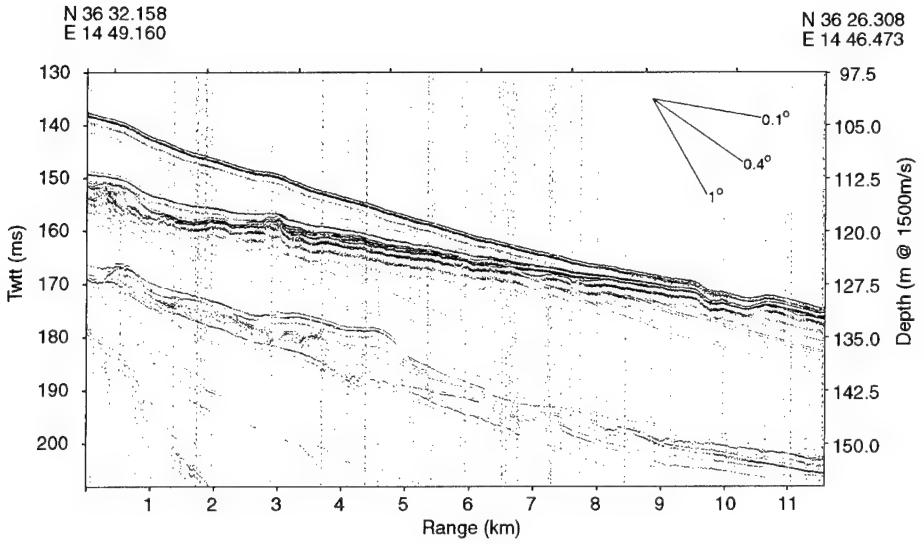

Figure 2 *Seismic reflection data of transect from Site 4 (0 km) to Site 1 (11 km). Site 5 is at 6.25 km. The vertical exaggeration is 100:1 and the inset shows the apparent slopes. Note that the angles of all the reflecting horizons are less than 1 degree. The base of the first sediment layer can be seen at Site 4 (0 km) at 150 ms two-way travel time (Twtt)*

2.1 Site 4

The water depth at Site 4 is 102 m and the bathymetry is locally very flat with a very small (~0.2°) seaward slope. A 6.8 m piston core[1] showed a very homogeneous silty clay throughout the upper 6.65 m with a porosity varying from 76% at 20 cm depth to 67% at 5.9 m. The bottom 0.15 m were sandy with large shell fragments.

Two short (1.2 m) gravity cores also showed the same silty clay material. Although the absolute values of the sound speed could not be ascertained[2], the data (see Fig. 3) indicate the presence of a sound speed gradient, estimated at 1.5 s^{-1} as shown in the dotted black line.

[1] The sediment was highly disturbed during handling and transport, thus sound speed measurements were unreliable.

[2] Insufficient water above the core was available for proper calibration for sound speed measurements. In addition, a multipath problem in the measurement system prevented reliable results.

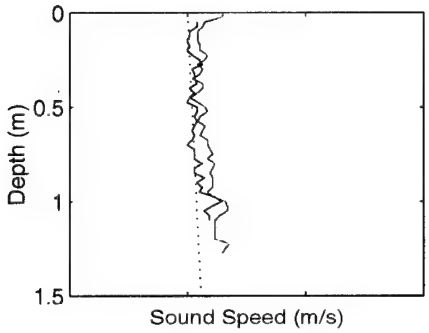

Figure 3 *Measurements (red and blue) from two gravity cores. The tick marks are 10 m/s and the dashed line is a sound speed gradient of 1.5 s^{-1}.*

2.2 Site 1

Site 1 lies at 128 m water depth; the seafloor is locally very flat. Sidescan data in this area shows a generally featureless flat bottom with faint lineations caused by dragnet fishing. Gravity coring at this site showed a silty-clay layer with a high sound speed gradient (see Fig. 4). Piston coring showed that below the silty clay layer there exists a thin sandy layer and then an extraordinarily coarse gravel layer extending for 2 m to the bottom of the core. Figure 5 is a photograph of the material found in the core catcher (about 3 m sub-bottom) and reasonably representative of the lower 2 m. It was remarkable to the author, given the size of the shells and cobbles, that the piston core penetrated so far. This may suggest that though coarse, the sediment is loosely packed.

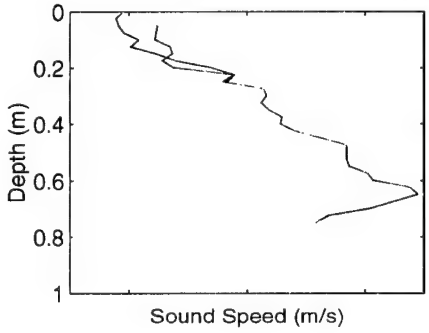

Figure 4 *Relative sound speed measurements (red and blue) from two gravity cores at Site 1. The tick marks are 10 m/s intervals. The two cores were separated by approximately 20m.*

Figure 5 *Photograph from contents in the core catcher at Site 1, showing large whole shells, shell fragments, pebbles, and cemented rock, in a muddy shelly gravel matrix. The coin in the foreground is 2.5 cm in diameter.*

2.3 Site 10

The water depth at Site 10 is 125 meters and the bathymetry is very flat. The core data at Site 10 showed an upper layer (~25 cm) of silty-clay, then a layer of clayey sand with shell fragments (~30 cm), then gravelly sand. Figure 6 provides the sound speed and density measurements.

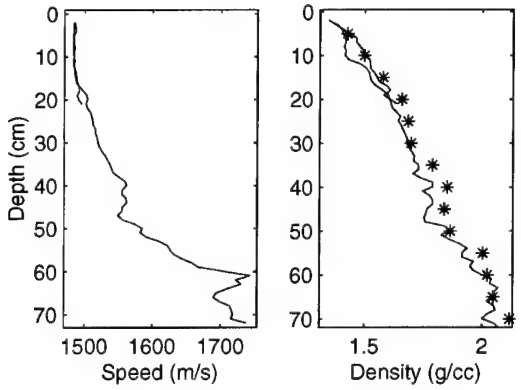

Figure 6 *Two core analyses (solid lines) at Site 10 from the multi-sensor core logger. The asterisks were measured using standard laboratory methods as a cross-check. The cores were separated by approximately 130 m.*

3
Reflection Measurements

3.1 Measurement Technique Overview

This technique was developed in order to extract very high resolution geoacoustic information from the seafloor. The measurement configuration uses a broadband source and a single hydrophone (see Fig. 7). It is a "local" technique in the sense that it samples a relatively small (a few hundred metres) region of the seafloor. This "local" attribute provides the opportunity to develop range-dependent geoacoustic models by making measurements at several sites (Holland, 2000).

The source employed in the experiments was either an EG&G Model 265 Uniboom or a Geoacoustics Model 5813B Boomer mounted on a catamaran at a nominal depth of 0.40 m. The source repetition rate was 1 pulse per second. The receiver consisted of a vertical array of which only the bottom hydrophone (~15 m above the bottom) was employed in the analysis. Although multiple phones could be used to increase the data coverage, the data from one hydrophone is sufficient to meet the analysis requirements. Data were sampled at 48 kHz with a low pass filter of 16 kHz and telemetered back to R/V *Alliance*. Details regarding the experiment design and data processing can be found in Holland and Osler (2000).

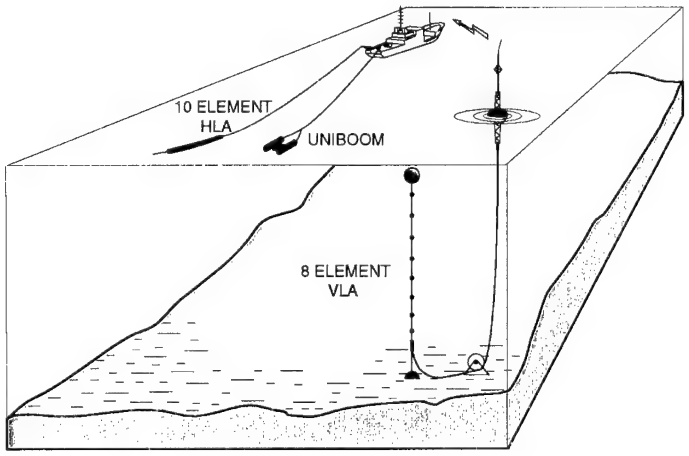

Figure 7 *Reflection experiment geometry, the data presented in this section is from a single hydrophone of the vertical array.*

3.2 Site 4 Data and Analysis

Figure 8 shows the raw time series reflection data mapped with a reducing velocity, *cr*,

$$t^2 - (range/cr)^2$$

so that arrivals traversing a path with an average velocity equal to that of the reducing velocity appear to be "flat" in range (i.e., independent of the reduced time). The weak reflection at the water-sediment interface, ~0.0062 s^2, is from the silty-clay layer. By windowing in time around this layer the reflection coefficient for the water-sediment interface can be calculated.

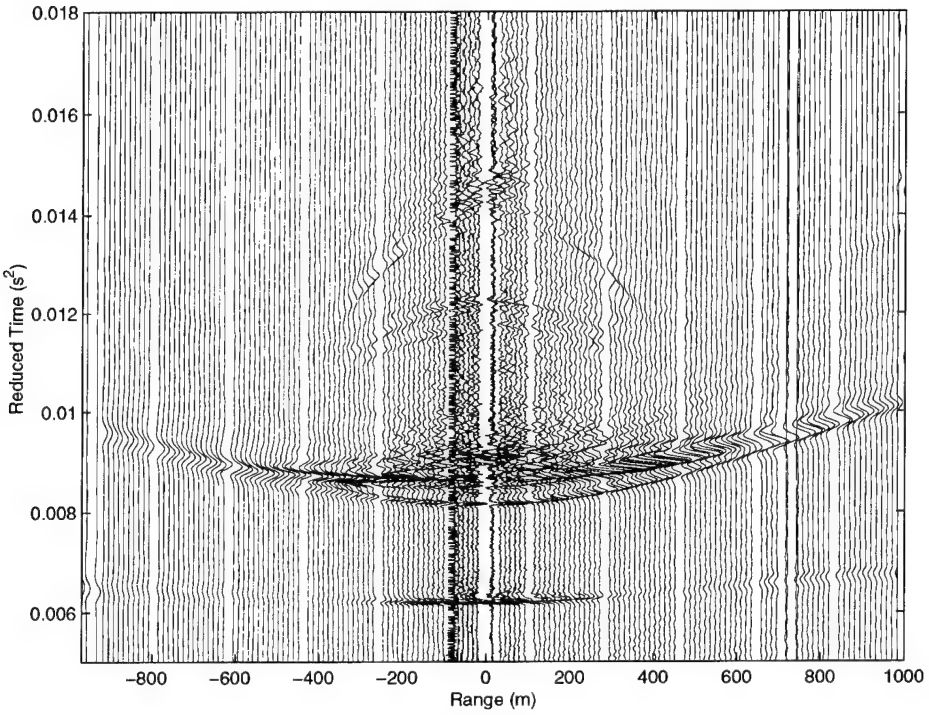

Figure 8 *Broadband bottom reflection time series data at Site 4 with a reducing velocity of 1511.9 m/s. Range is relative to the location of the hydrophone. The water-sediment interface reflection occurs at 0.0062 s^2.*

Figure 9 shows the processed reflection loss data (x) for the water-sediment interface. One of the salient features of these data is that the water-sediment interface is nearly completely acoustically transparent; above grazing angles of 10°, 99% of the energy is transmitted into the sediment. Thus, the sub-bottom sediment structure will tend to govern the reflection and scattering characteristics. The other salient feature in the data is

the presence of the angle of intromission, the angle where the reflection coefficient approaches zero. Using a simple but robust geoacoustic inversion method based on the angle of intromission and the normal incidence reflectivity (see Holland, 2001), the sound speed and density of the silty-clay is estimated at 1480 m/s and 1.32 g/cc[3]. These values are in excellent agreement with the time-domain inversion discussed in the next section. They are also in agreement with the closest high quality core data of 1483 m/s and 1.346 g/cc (2 cm depth) at Site 10.

The peak of the reflection loss at the angle of intromission is very sensitive to attenuation, suggesting that attenuation can also be extracted. However, other sediment properties like interface roughness, ultra fine-scale layering and volume can also control the small but finite loss at that angle.

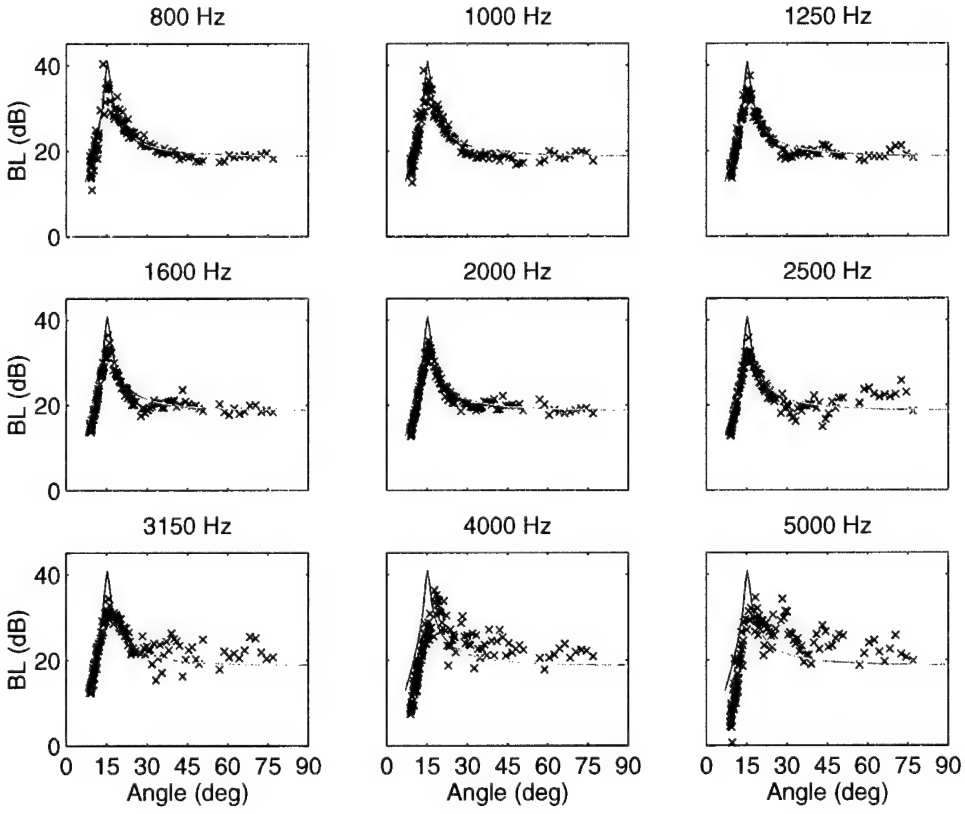

Figure 9 *Measured 1/3 octave bottom reflection loss (x) from the water-sediment interface of Site 4 with the model results from the geoacoustic inversion (red line).*

[3] The bottom water sound speed and density are 1511 m/s and 1.029 g/cc, respectively.

Model-to-data comparisons using the inversion results are shown in Fig. 9 with a fitted effective attenuation of .07 dB/m/kHz. The effective attenuation value is useful in defining the absolute upper bound for intrinsic attenuation, which for this sediment type is expected to be one order of magnitude smaller (e.g., Hamilton, 1980). The model predictions (reflection at a halfspace) are frequency independent. Note that the fit between the model and the data are excellent from 800-2000 Hz , but above 2000 Hz the data show definite dependencies on frequency. The frequency dependence of the data is indicative of the presence of ultra fine-scale layering and/or volume inhomogeneities. The analyses in Annex A indicate that fine-scale layering is the main cause of the frequency dependence and also explain the reflection loss at the angle of intromission.

Time domain analysis provides an estimate of the interval velocities for each of the sediment layers. Figure 10 shows the raw time series data along with the reflecting horizon picks (dashed lines). Figure 11a gives the resulting sediment interval sound speeds. The average sound speed in the top 10 m is 1490 m/s and using the 1.5 m/s sound speed gradient observed in the core data (Fig. 4), the interface sound speed of 1482.5 m/s agrees extremely well with the intromission inversion of 1480 m/s.

The arrival structure in observed in the data from 0.008-0.009 s^2 indicates a complex layering sequence that is not well-resolved by the transmit pulse. For example, the time domain analysis shows that the first two sediment layers are 8.4 m and 1.8 m thick respectively with sound speeds of 1490.1 m/s and 1490.5 m/s. However, observation of the strong reflection at 8.4 m sub-bottom (0.008 s^2) in Fig. 10 clearly indicates that there must be a high impedance contrast at that boundary (8.4 m sub-bottom). Moreover, the piston core data showed a sandy/shelly layer at the base of the core which almost certainly corresponds with this reflector. Co-registration with the acoustic data indicates that there was about a 20% compression/loss of material in the piston core which is not unreasonable for this kind of device. Thus, the relatively low interval velocity of layer 2 simply indicates that most of the 1.8 m is the same material as layer 1 with a very thin high speed layer at the top. The important summary observation is that the sound speed for these closely spaced layers are difficult to estimate using the time domain method. However, the frequency domain data (reflection loss) can provide the geoacoustic properties on the closely spaced layers such as these.

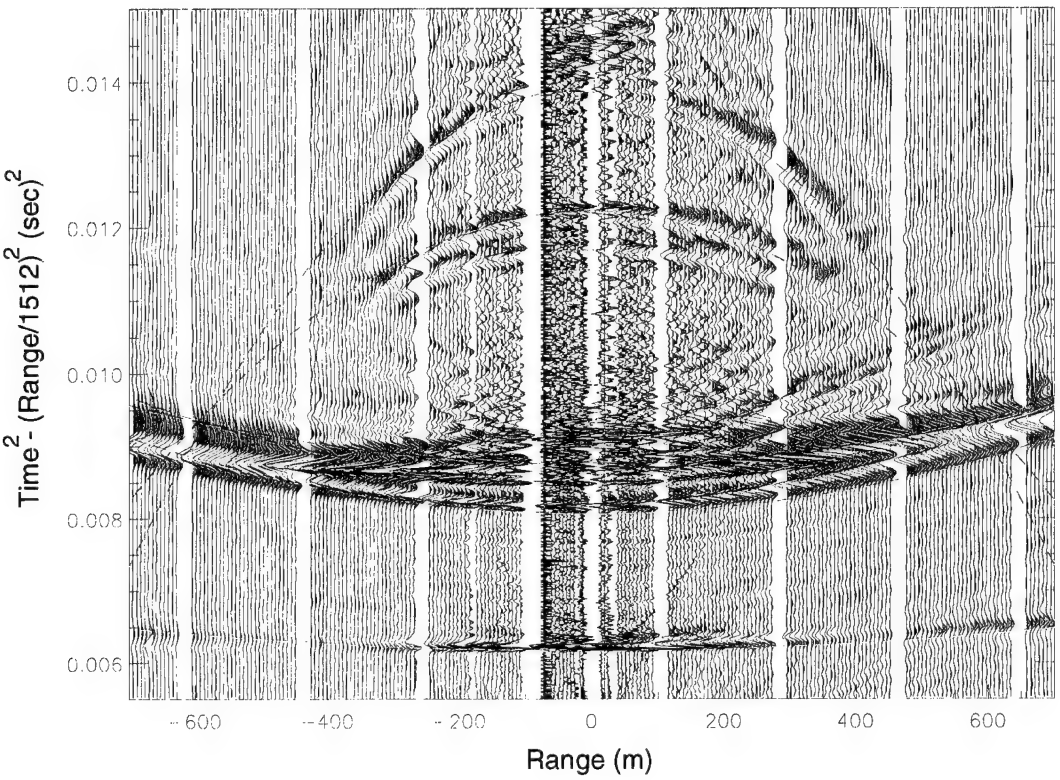

Figure 10 *Site 4 raw reflection data with horizon picks (dashed red hyperbolae). The reflection from the water-sediment interface is at about 0.006 s^2.*

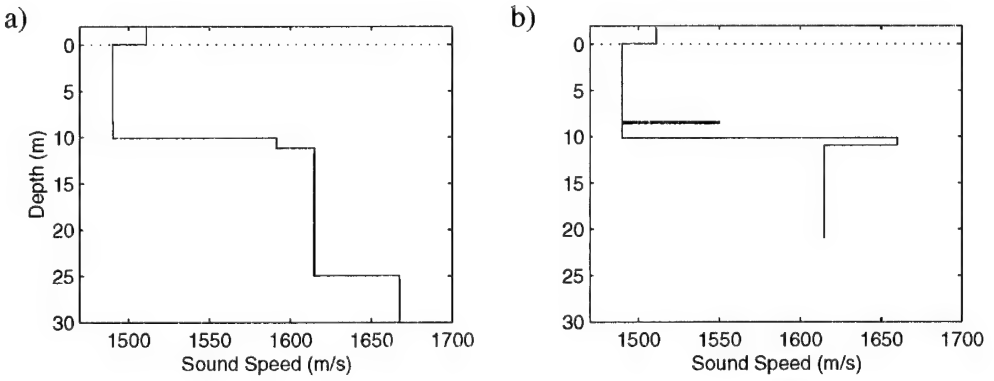

Figure 11 *Site 4 sediment sound speed from time domain analysis a) using hyperbolae fits to the main reflecting horizons; b) modified profile after frequency domain analysis.*

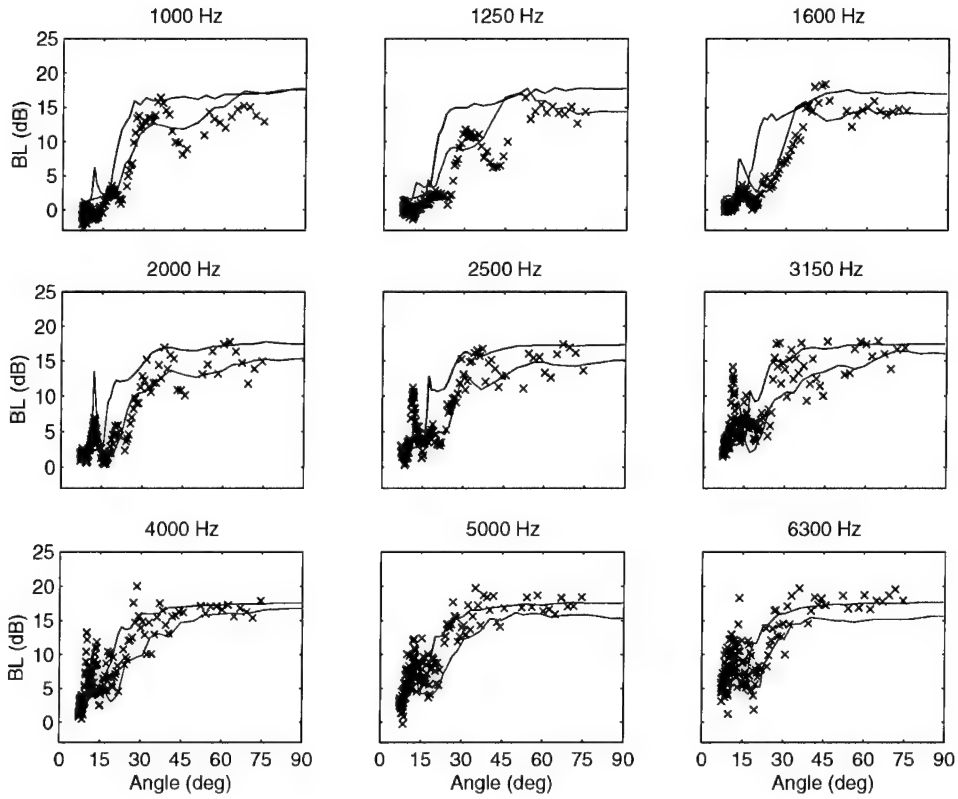

Figure 12 *Bottom reflection loss data (x) from Site 4 with the time domain (blue) and modified time domain geoacoustic properties (red).*

The reflection loss data for the upper 20 m of the sediment column are shown in Fig. 12. Also shown are the predictions using the geoacoustic properties derived from the time domain data (blue line). The model fits the measurements in a general sense, but there are clues in the reflection data that can improve the geoacoustic model. For example, using the apparent critical angle of the data (~ 25°) the second layer sound speed was estimated at 1660 m/s. Also, the peak in the reflection coefficient at about 13° (2-3 kHz) confirms the existence of, and provides estimates of the properties for the high-speed layer at 8.4 m. The reflection predictions (Fig. 12 red line) using the modified geoacoustic properties (see Fig. 11b) are in better agreement across angle and frequency. It is believed that scattering from the layer at ~10 m sub-bottom explains why the data have a generally higher loss than the model at high frequencies. Note also, that there is greater variability in the high frequency data, which is also indicative of scattering.

Including the sound speed gradient in the first sediment layer has a negligible effect on the reflectivity and so for simplicity was not included in the geoacoustic properties. The

accompanying density gradient can not be ignored; it has the effect of changing the impedance contrast at the base of the silty-clay layer. The geoacoustic properties for Site 4 are given in Table 1. The basement attenuation value has considerable uncertainty, since the reflection loss is not sensitive to that parameter.

Table 1 *Geoacoustic properties for Site 4.*

Thickness (m)	Sound Speed (m/s)	Density (g/cc)	Attenuation (dB/m/kHz)
8.4	1490.	1.32-1.5	0.01
0.2	1550	1.7	0.05
1.6	1490.	1.6	0.02
0.8	1660	1.80	0.2
-	1615	1.70	0.2

3.3 Site 1 data and analysis

Figure 13 shows the raw time series reflection data at Site 1. The relatively weak water-sediment reflection occurs at .0095 sec^2 and two strong reflectors follow very close in time at about 0.0099 sec^2.and 0.0101 sec^2. No other reflecting horizons[4] are apparent until about 30 m sub-bottom (not shown) where there is a relatively weak low-frequency reflector.

The sediment sound speed profile obtained from the time domain analysis in the upper few metres is shown in Fig. 14. Note that the first layer sound speed is essentially identical to that at Site 4, indicating the same kind of surficial sediment at the two sites. Due to the closely spaced sub-bottom layers, it was difficult to accurately pick the hyperbolae for the second layer. However, the frequency domain data (reflection loss) can provide information on this layer.

Figure 15 shows the measured reflection loss (x) at this site. The blue curve shows the predictions using the sound speed profile from Fig. 14a which do not agree particularly well with the measurements (almost certainly due to inaccuracies in the second layer sound speed). Using the location of the critical angle at high frequency (5 kHz) as a guide, the sound speed of the second layer was estimated to be 1780 m/s. Oscillations observed in the high angle (> 45°) and 1-2 kHz data suggested that the second layer thickness was about a factor of 2 too large. The modified sound speed profile (red dashed curve of Fig. 14b) fits the measured reflection data considerably better (see red curve in Fig. 15).

[4] The feature on the positive ranges at about 0.0105 sec^2 and 400 m offset is a reflection from the tow ship and not a reflector.

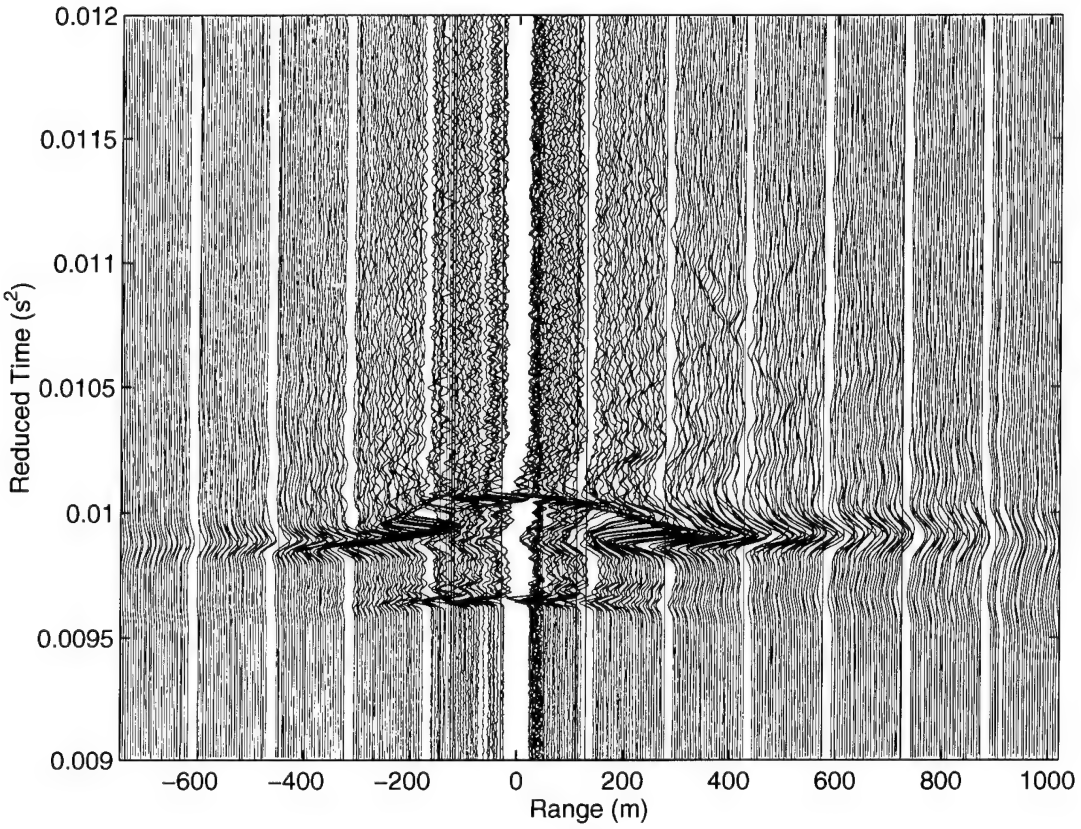

Figure 13 *Broadband reflection time series data at Site 1 with a reducing velocity of 1512.8 m/s. The water-sediment interface reflection is at .0095 sec²*

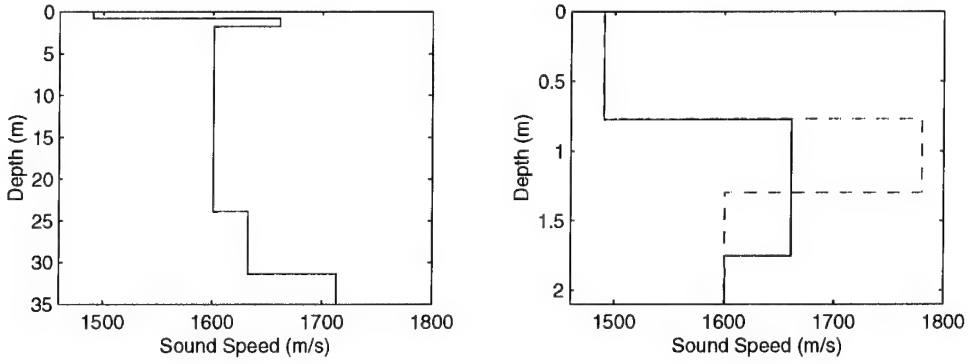

Figure 14 *Sediment sound speed profile at Site 1. The solid blue curve is from the time domain analysis, the red line is from the frequency domain (reflection analysis).*

However, the fit to the low angle data in Fig. 15 require an unrealistically large attenuation of 0.1 dB/m/kHz in the first (silty-clay) layer. It is unrealistic from the standpoint that it is a factor of 10 higher than the 1st layer attenuation at Site 4 (which has the same sound speed); it is greater than the effective attenuation from the similar sediment type at Site 4, and much higher than the literature (e.g., Hamilton, 1980) would predict for a silty-clay. In connection with this, note that the predictions do not match the data at high frequency (4-6 kHz) high angle (> 45°) and the bias in the model vice the data increases with increasing frequency. A probable explanation for both these effects is scattering due the large inclusions as shown in Fig. 5.

In order to estimate the effect of scattering in the second layer, several model predictions were made including scattering at the second layer interface (using the Kirchhoff approximation). Figure 16 compares the no scattering case (red) with an *rms* roughness of 3.5 cm (blue); both predictions use the same attenuation found at Site 4 (0.01 dB/m/kHz). The frequency dependence of the low and high angle predictions indicates that scattering plays an important role in the reflection process. However, noting the different low-angle (< 30°) dependence of the model and data at 5-6 kHz, volume scattering rather than interface scattering may be the actual mechanism involved. Table 2 provides the geoacoustic properties at this site.

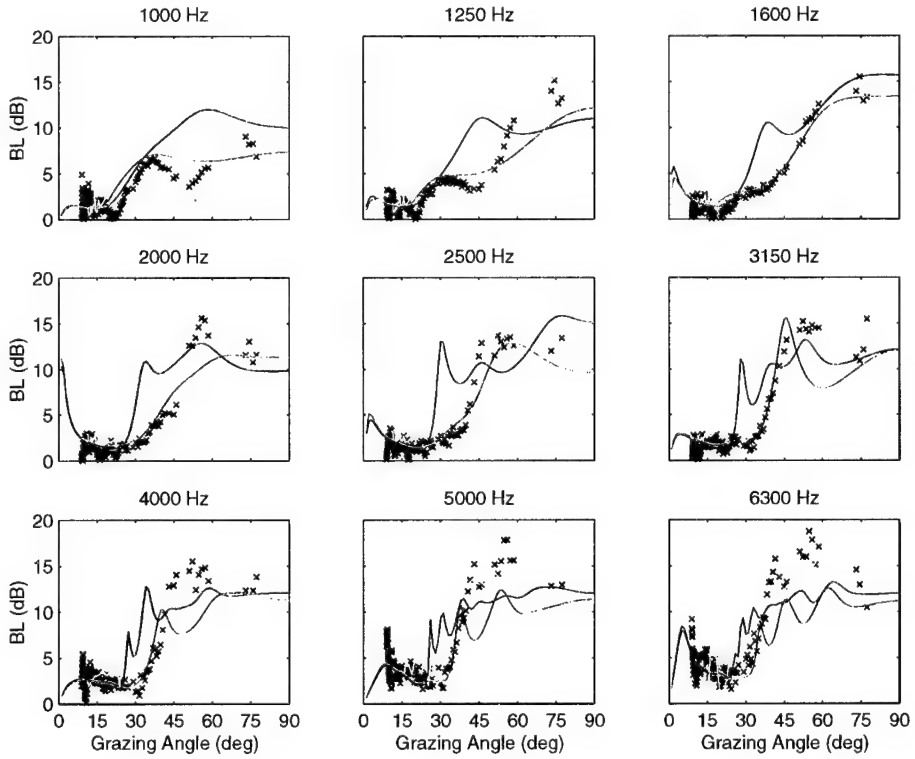

Figure 15 *Comparison of Site 1 measured reflection loss (x) with model using layer structure from time domain analysis (blue) and modified time domain analysis (red).*

Table 2 *Geoacoustic properties for Site 1*

Thickness (m)	Sound Speed (m/s)	Density at top (g/cc)	Attenuation (dB/m/kHz)	RMS roughness (cm)
0.8	1490.	1.32	0.01	0
0.5	1780	1.85	0.2	3.5
-	1600	1.62	0.2	--

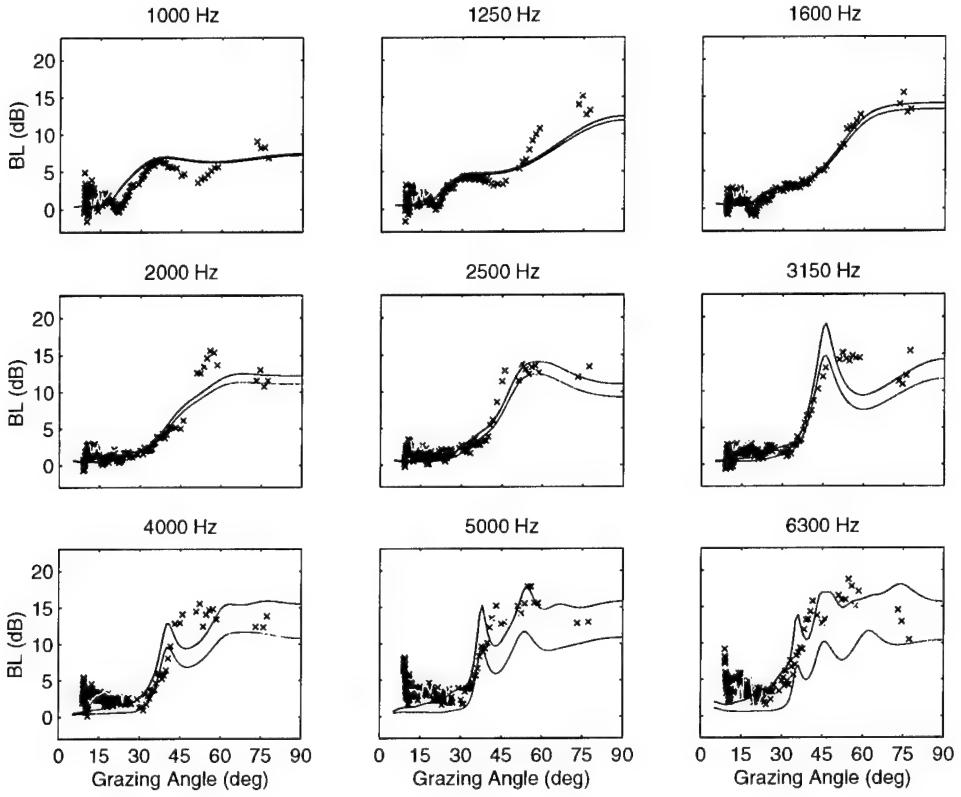

Figure 16 *Comparison of Site 1 measured reflection loss (x) with model using geoacoustic properties from Table 2 with roughness (blue) and without roughness (red).*

3.4 Summary of reflection results

In summary, the Malta plateau appears to have a blanket of surficial silty-clay with uniform geoacoustic properties but spatially variable thickness. The thickness decreases seaward (see Fig. 2). Below the silty-clay layer there are several thin (tens of centimetres) high-speed layers. Below the thin layers, there is a thick layer of ~ 1600 m/s that effectively forms the acoustic basement at these frequencies. From the core data at Site 1,

this sandy layer has large inclusions of shells, shell fragments, and pebbles. The high speed layer may also have large inclusions. There appears to be significant scattering at this layer, especially apparent at Site 1. There is no independent data to indicate that the inclusions also exist at Site 4, however, this seems to be implied inasmuch as the velocity of that layer is almost identical (less than 1% difference) between the two sites. Analysis of the reflection data provide sound speed, density, attenuation and layer thickness estimates of the sedimentary structure required for scattering predictions.

4

Scattering measurements

In this section the scattering measurements are presented and interpreted in light of the geoacoustic properties obtained from the reflection analysis.

4.1 Measurement technique overview

Like the reflection technique, the scattering measurements are "local", i.e., yield scattering strength in a relatively small (several 100 m) radius. The technique allows not only measurement of bottom scattering strength but also provides information on the scattering mechanism (i.e., interface or sub-bottom volume scattering). Knowledge of the scattering mechanism is important because it can serve as a key for predicting the frequency dependence of the scattering. Details of the measurement and analysis technique are given in Holland et al (2000).

The scattering mechanism information is contained in the beam time series. Figures 17 and 18 show the various multipath orders and the resulting arrival structure. This report will focus on the backscattering branch, branch *a*. Deviations from the predicted arrival structure of branch *a*, including time delays, arrival elongation, or the addition of other branches directly point to the existence of sub-bottom scattering.

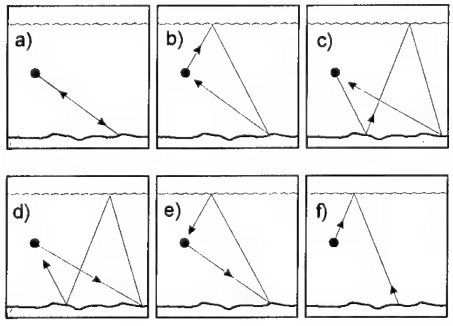

Figure 17 *Bottom scattering multipaths*

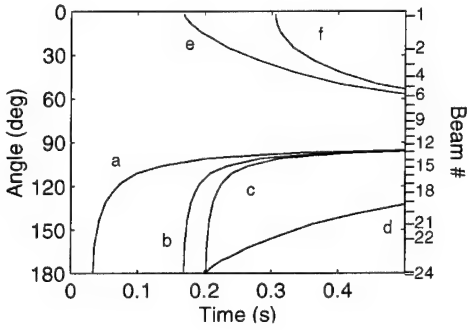

Figure 18 *Vertical arrival structure for multi-paths of Fig. 17. 180° is toward seafloor*

4.2 Site 10 data and analysis

Site 10 is on the eastern edge of the Malta Plateau, just 1.5 km west of the Ragusa ridge, in 126 m of water depth. This site was selected to examine the difference in scattering strength between the central Plateau (Site 1) and its eastern edge.

The beam time series data are shown in Fig. 19 along with modelled arrival branches (white dashed lines) whose geometrical meaning can be understood from Fig. 17 and Fig. 18. Note that there is no time delay between the modelled and measured scattering branch *a*; moreover modelling (not shown) indicates that there is no substantial time spreading of this branch. These two facts indicate that the scattering is coming from the upper 10 m of sediment (i.e., the limits of the pulse/beam resolution spatial resolution). The core data show a high-speed layer sandy gravel layer at 0.60 m sub-bottom. This layer is probably the dominant mechanism giving rise to the scattering.

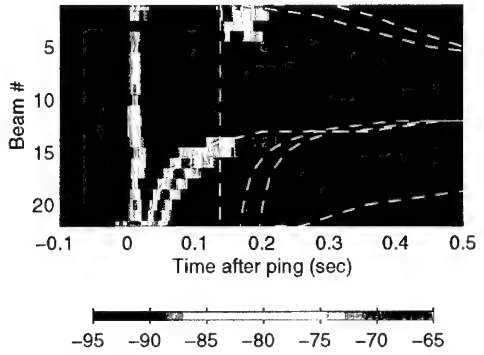

Figure 19 *Averaged (10 pings) beam time series from 3600 Hz bottom scattering at Site 10. The quantity plotted is received level re 1 uPa^2/s/Hz. The direct blast is seen just after 0 seconds across all the beams and the surface reflection is observed at 0.14 sec. The vertical white dashed line at 0.1 seconds is the model result for the surface reflection; the other white dashed lines are model results for the various bottom scattering paths. No delay between the modelled and measured arrivals is observed indicating that the scattering is coming from at or near the sediment surface.*

Processed backscattering strength as a function of angle and frequency are shown in Fig. 20. For comparison with a common standard, the data are parameterized by a Lambert coefficient, which is shown in the dotted line. Note that the scattering strength at Site 10 is very small below 1800 Hz .

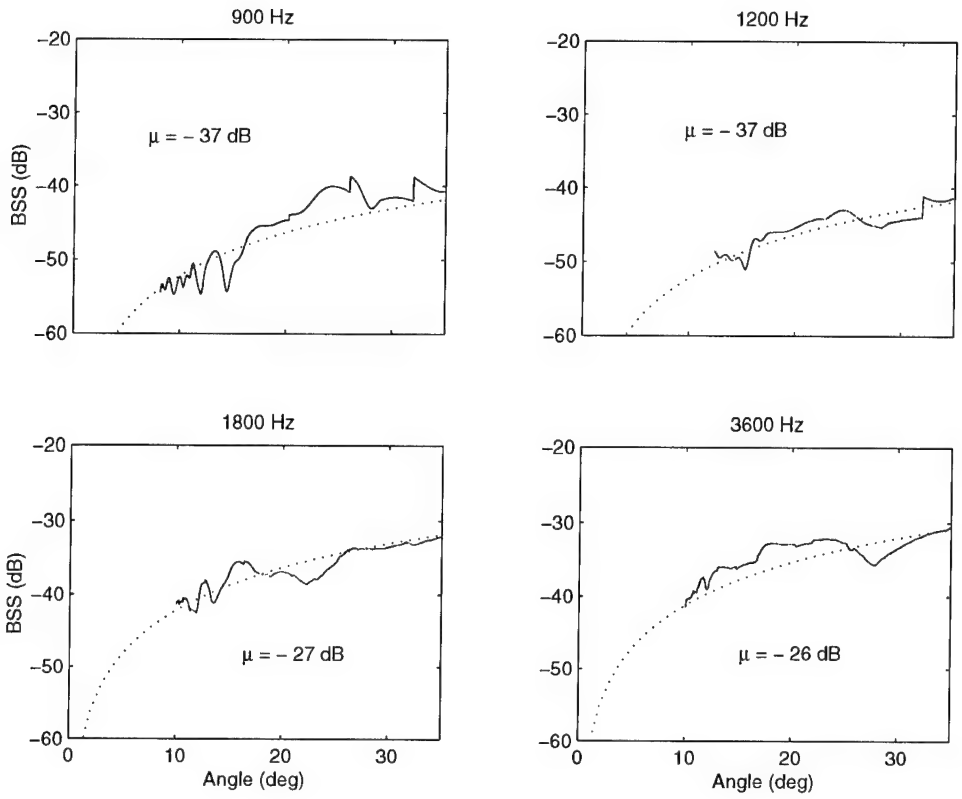

Figure 20 *Direct path Scattering strength data (red) and fits (dashed line) at Site 10 on the Malta Plateau. Data processing was difficult at this site because of the very low scattering strengths at 1200 Hz . Thus, the 1200 Hz results were obtained using only 1 beam for the scattering strength integration; integrating over several beams gives poor results because of apparent contamination from normal incidence sub-bottom contributions.*

4.3 Site 4 data and analysis

The reflection analysis at Site 4 shows that the upper 10 m of sediment is silty-clay with a sound speed less than that of the overlying water column. The presence of the surficial silty-clay layer has an important effect on the scattering as well as on the reflection.

Figure 21 shows the beam time series from the bottom scattering measurement. The predicted backscattering branch (white dashed curve) can be observed at about 0.4 seconds past the direct blast on beam 22. The measured backscattering branch (branch *a* in Fig. 17 and Fig. 18) arrives ~14 ms later than the prediction. This time delay indicates that the scattering is coming not from the water-sediment interface, but rather from a horizon about 10 m sub-bottom. The time delay can also be clearly seen on bistatic

branch *b* in beams 20-22. The reflection data showed a high-speed layer at about 10 m (see Fig. 8 and Fig. 11), which we now observe to be the dominant scattering layer in this environment. Note also, that the width of the branch is about the same as at Site 10 (Fig. 19) which means that deeper layers are not contributing (significantly) to the scattering.

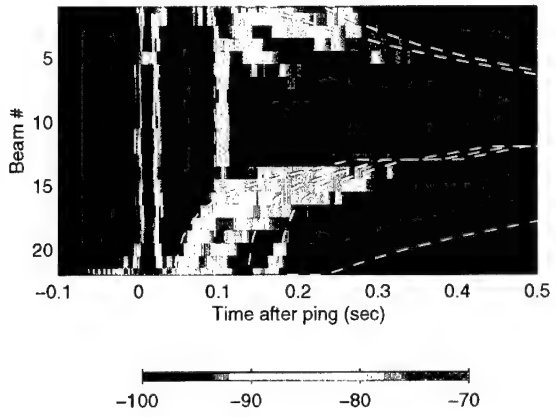

Figure 21 *Averaged (10 pings) beam time series from 3600 Hz bottom scattering at Site 4. The vertical white dashed line at 0.1 seconds is the model result for the surface reflection; the other white dashed lines are model results for the various bottom scattering paths. The delay between the modelled and measured arrivals indicates that the scattering comes from about 10 m below the water-sediment interface.*

Processed backscattering strength as a function of angle and frequency are shown in Fig. 22. For comparison with a common standard, the data are parameterized by a Lambert coefficient, which is shown in the dotted line. Modelling results are shown in the next section. The scattering strength at Site 4 is very small below 3600 Hz .

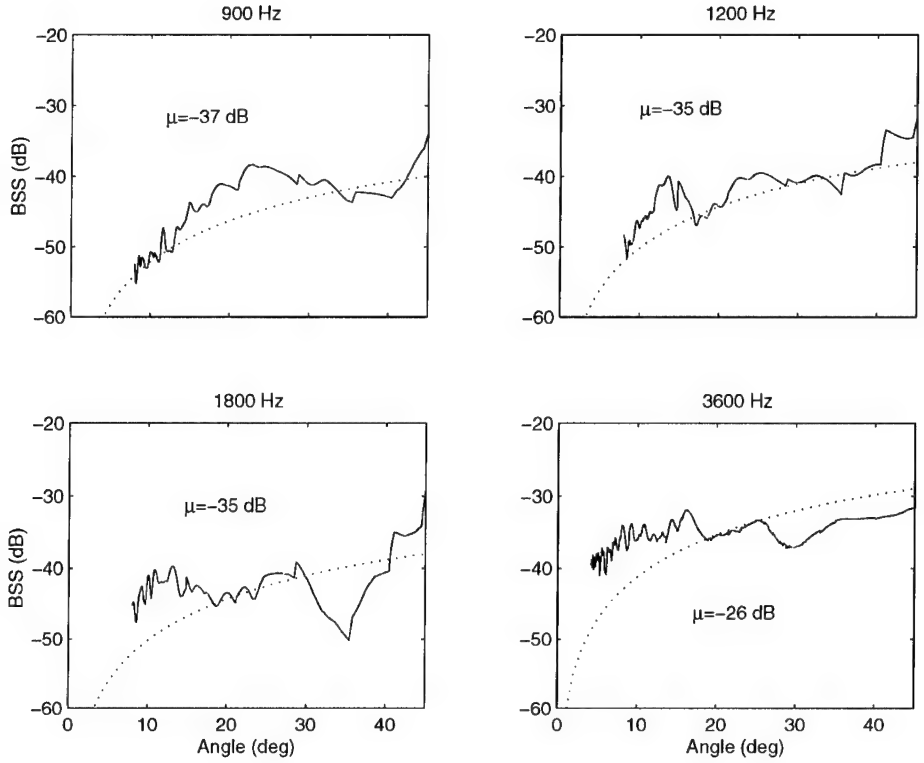

Figure 22 *Direct path scattering strength data (red) and fits (dashed line) at Site 4 in the Malta Plateau. Data processing was difficult at this site because of the very low scattering strengths. The 1200 and 1800 Hz data used only 1 beam for the scattering strength integration; integrating over several beams gave poor results because of apparent contamination from normal incidence sub-bottom contributions. The peak at about 15° at 1200 Hz is an artifact due to the sea surface reflection.*

4.4 Site 1 Data and Analysis

The reflection analysis at Site 1 showed a strongly reflecting/scattering layer 0.8 m below the water-sediment interface. In agreement with that analysis, the beam time series at Site 1 (Figure 23) show no measurable[i] time delay between the modeled and measured scattering arrivals. There is, however, a significant spread in the width of branch *a* as compared to Site 10. The presence of large cobbles and shells (see Figure 5) in layer 3 suggest that volume scattering in layer 3 is the cause of the spreading of the branch in beam space.

In order to show the effect of volume scattering on beam broadening, Figure 24a and b show modeled results of the beam time series for volume scattering and interface scattering respectively. The volume scattering results assume a very small attenuation in layer #3 (0.01 dB/m/kHz) and distribute the scatterers from 1.5 m to 22 m sub-bottom. Comparison of the modeled arrival structure with the measured data of Figure 23 appears to confirm the presence of sub-bottom volume scattering. The scattering contributions are probably limited to the upper 10 meters of sediment.

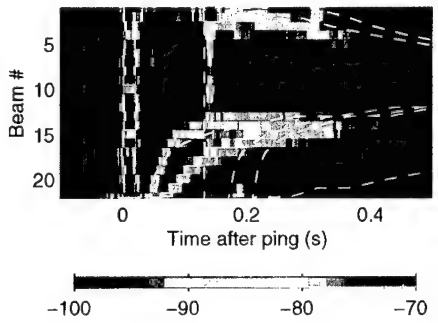

Figure 23 *Averaged (10 pings) beam time series from 3600 Hz bottom scattering at Site 1. No delay between the modeled and measured arrivals is observed indicating that the scattering is coming from at or near the sediment surface. The temporal/beam spreading of the arrivals indicates that the scattering is also coming from deeper in the sediment column.*

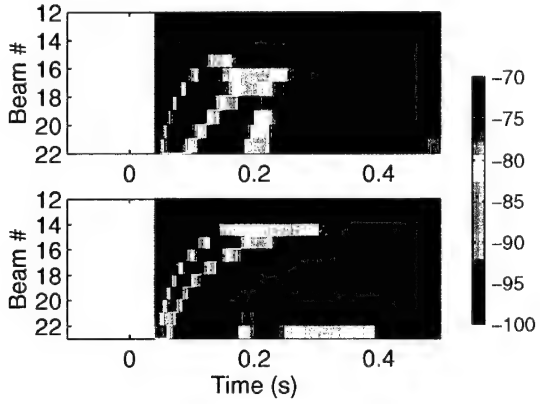

Figure 24 *Direct Modeled results of the beam time series at Site 1 assuming a) volume scattering from 1.5-22 meters sub-bottom and b) interface scattering. Comparison with* ***Figure*** *indicates that the scattering arises from the sub-bottom volume inhomogeneities.*

the water-sediment interface. In agreement with that analysis, the beam time series at Site 1 (Fig. 23) show no measurable[5] time delay between the modelled and measured scattering arrivals. There is, however, a significant spread in the width of branch *a* as compared to Site 10. The beam-time spread indicates that there are scattering contributions coming from near the sediment interface down to about 20 m sub-bottom. The reflection time series data show the first two reflecting horizons at 0.8 m and at 22 m sub-bottom (the latter can be seen in Fig. 2 at 150 m depth). What is remarkable is that the scattering is coming from so deep in the sediment (~ 50 wavelengths).

Processed backscattering strength as a function of angle and frequency are shown in Fig. 25. Note the overall similarity to the bottom scatter data at Site 4. The salient difference between the two sites is that the increase in scattering strength with frequency is weaker at Site 4 than at Site 1, which is consistent with Site 4 having a thicker silty-clay layer. The other difference between the two sites is the thin high speed layer at Site 4, absent at Site 1.

In order to more clearly show the effect of the silty-clay thickness on the scattering strength, modelling was performed using sediment properties obtained from the reflection data (see Tables 1 and 2). Figure 26 shows the modelled and measured data at Sites 1 and 4. The model fit the data quite well. With a silty-clay attenuation of 0.01 dB/m/kHz, the model indicates that the attenuation accounts for about 2 dB of the modelled difference between the two sites and the presence of the thin 0.2 m layer accounts for another 2 dB.

[5] The uncertainty associated with the source depth, receiver depth, and water depth are of order a metre, i.e., insufficient for determining departures from the predicted arrival structure of that order.

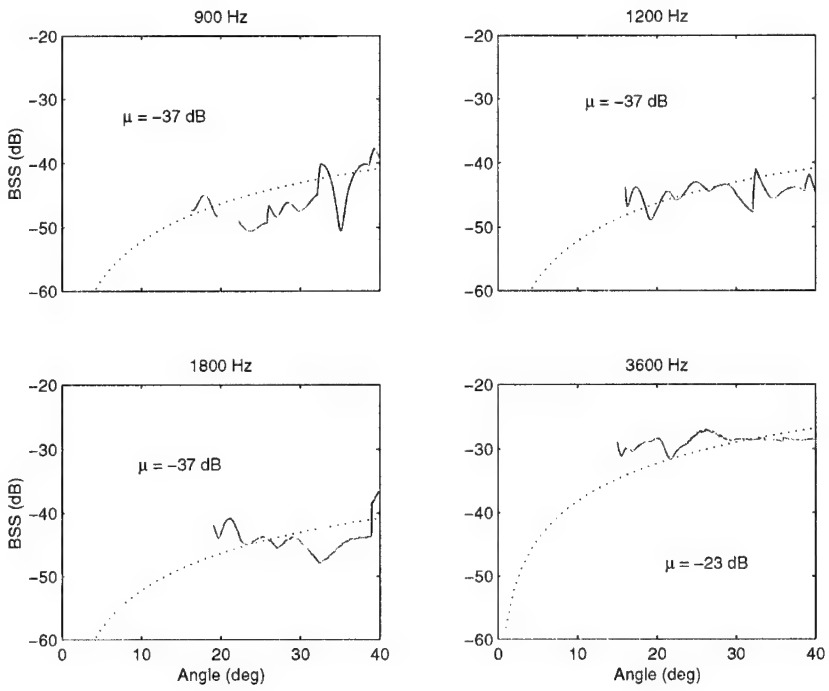

Figure 25 *Direct path scattering strength data (red) and fits (dashed line) at Site 1 in the Malta Plateau. Data processing was somewhat difficult at this site due to the very low scattering strengths. The 1200 and 1800 Hz data used only beam for the scattering strength integration; integrating over multiple beams gave poor results because of apparent contamination from normal incidence sub-bottom contributions.*

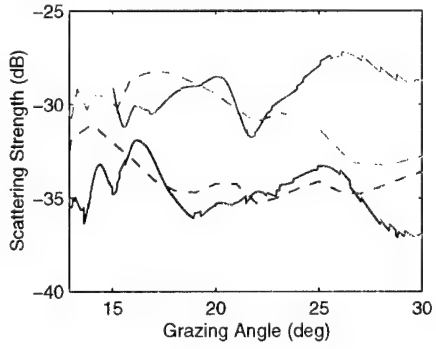

Figure 26 *Measured and modelled bottom scattering strength at Sites 1 and 4 showing the effect of the range-dependent thickness of the upper silty-clay layer at 3600 Hz . Measured (solid red) and modelled (dashed magenta) Site 1 scattering are higher than the Site 4 measurements (blue solid) and model (cyan) in part because the upper silty-clay layer is thinner, hence reducing the attenuation.*

5
Summary and conclusions

In previous studies of acoustic interaction with the seabed, often only the quantity of immediate interest (reflection or scattering) is measured. Measuring both quantities in a coupled manner, provides the opportunity to understand the seafloor geoacoustic properties and physical mechanisms more completely. In particular, the geoacoustic properties obtained from the reflection data provides insight into the scattering and its site-to-site variability. The complexity of the seafloor suggests the need for sub-bottom scattering models that include layering.

The coupled analysis provided substantial detail about the mechanisms involved in both the reflection and scattering. Acoustic interaction with the seafloor on the Malta plateau is dominated by reflection and scattering from the sub-bottom rather than the sediment interface. The first sediment layer, silty-clay, is nearly acoustically transparent and contributes very little to the reflection and scattering process, except as a lens, modifying the angular content of the incident field on the sub-bottom layers. It appears to have uniform geoacoustic properties across the Plateau, but variable thickness, from roughly 1-10 meters. The dominant scattering mechanism at Sites 4 and 10 appear to be the high speed layers immediately below the silty-clay layer. At Site 1, there is evidence of scattering from the upper 10 meters of the seabed at 3600 Hz.

Acknowledgements

I would like to thank the scientific staff and captain aboard the NATO R/V *Alliance* during the cruises in which these data were collected. Special thanks to John Osler who developed the software for the time domain inversion of the reflection data and to Piero Boni who managed the data acquisition with energy and expertness.

References

Hamilton, E.L. Geoacoustic modeling of the seafloor. *Journal of the Acoustical Society of America*, **68**, 1980:1313-1339.

Hines, P.C. Theoretical model of acoustic backscatter from a smooth seabed. *Journal of the Acoustical Society of America*, **88**, 1990:324-334.

Holland, C.W., Osler, J. High resolution geoacoustic inversion in shallow water: A joint time and frequency domain technique. *Journal of the Acoustical Society of America*, **107**, 2000:1263-1279.

Holland, C.W., Neumann, P. Sub-bottom scattering: a modeling approach. *Journal of the Acoustical Society of America*, **104**, 1998:1363-1373.

Holland, C.W., Hollett, R., Troiano, L. A measurement technique for bottom scattering in shallow water, *Journal of the Acoustical Society of America,* **108**, 2000:997-1011.

Holland, C.W. Regional extension of geoacoustic data. *In*: Chevret P., Zakharia, M.E., editors. Proceedings of the Fifth European Conference on Underwater Acoustics, ECUA 2000 Lyon, France, 2000:793-798.

Holland, C.W. Direct observation of the angle of intromission in marine sediments, 2001.

Ivakin, A.N. Sound scattering by random inhomogeneities in stratified ocean sediments, *Soviet Physics Acoustics*, **32**, 1986:492-496.

Jackson, D.R., Winebrenner, D.P., Ishimaru, A. Application of the composite roughness model to high frequency bottom backscattering. *Journal of the Acoustical Society of America*, **79**, 1986:1410-1422.

LePage, K.D., Schmidt, H. Spectral integral representations of volume scattering in sediments in layered waveguides, *Journal of the Acoustical Society of America*, **108**, 2000:1557-1567.

Mackenzie, K.V. Bottom reverberation for 530 and 1030 cps sound in deep water, *Journal of the Acoustical Society of America*, 1961,**33**, 1498-1504.

Mourad, P.D., Jackson, D.R. A model/data comparison for low frequency bottom backscatter, *Journal of the Acoustical Society of America*, **94**, 1996:344-358.

Tang, D.J., Frisk, G.V. Spectral parameterization of scattering from a random ocean bottom. *Journal of the Acoustical Society of America*, **92**, 1992:2792-2799.

Yamamoto, T. Acoustic scattering in the ocean from velocity and density fluctuations in the sediment. *Journal of the Acoustical Society of America*, **99**, 1996:866-879.

Annex A
Modelling of fine-scale near surface layering

In Fig. 8 it was observed that the halfspace model did not fit the measured reflection loss data above 2 kHz. In this annex, an explanation is advanced assuming the presence of fine-scale layering.

In Fig. 8, note that from 4-5 kHz, the low angle data (below the angle of intromission) are shifted to higher angles relative to the halfspace predictions. This indicates that the high frequencies "see" a lower sound speed and/or density than the low frequencies. The simplest explanation is that there is a surficial layer with a lower sound speed. Note also, that at high frequencies, the high angle (> 45°) reflection data have a higher loss than the low frequencies, which is also consistent with a surface layer of lower sound speed and density.

Figure A1 shows the data predictions using a 10 cm surficial layer of 1470 m/s, 1.28 g/cc and 0.01 dB/m/kHz (see Table A1). The presence of this layer seems to explain 1) the increase in reflection at high frequencies, 2) the increase of the angle of intromission with increasing frequency , and 3) the reflection loss at the angle of intromission without resorting to large attenuations. The one aspect it does not explain is the presence of oscillations in the data above the angle of intromission, e.g. apparent at 5 kHz from 2-60°.

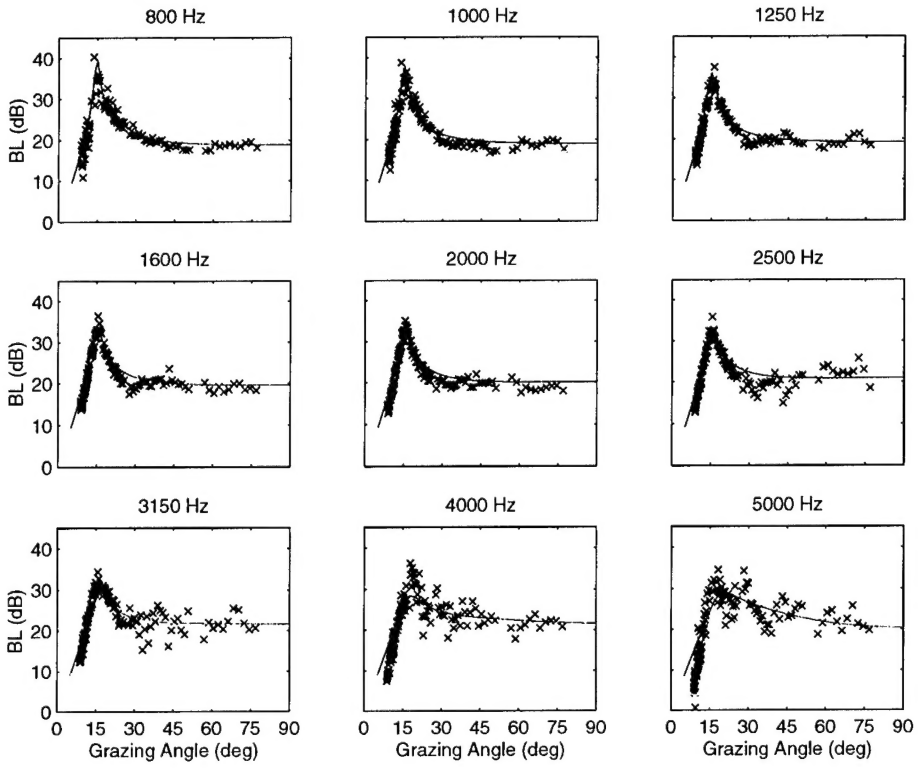

Figure A1 *Measured reflection loss (x) with model including at 10 cm surface layer. Note the shift in the modelled angle of intromission at high frequencies that is consistent with the data. Note also the improved fit of the high angle data relative that of Fig. 8.*

The oscillations at 4-5 kHz are presumed to come from layering. Figure A2 shows the predictions using a 3-layered bottom of Table A2. Note that at 5 kHz, the predicted oscillations agree reasonably well with the measured data. While the oscillations do not perfectly match the data, the similarity of the predicted oscillatory structure to that measured give credence to the hypotheses that ultra fine-scale layering

- is responsible for the high frequency departure from the half-space predictions, and
- controls the reflection loss at the angle of intromission.

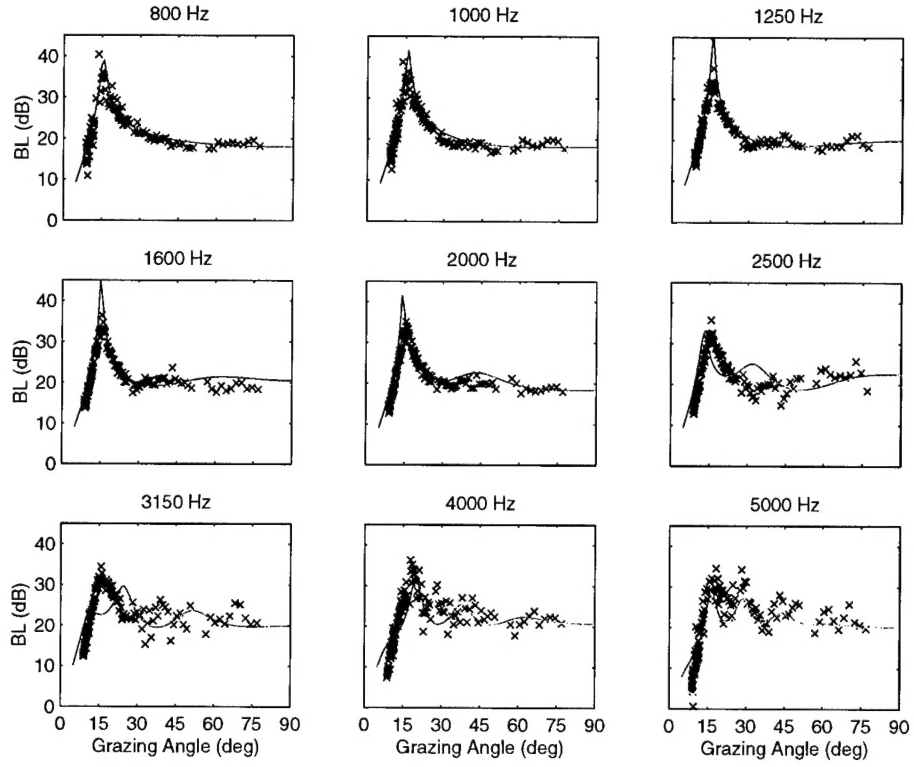

Figure A2 *Measured reflection loss (x) with model including at 10 cm and fine-scale near surface layering. Note that the oscillation structure in the model is similar to that in the data, indicating that the data oscillations are probably a resonance due to fine-scale layering.*

Table A1 *Geoacoustic properties for Fig. 26.*

Thickness (m)	Sound Speed (m/s)	Density (g/cc)	Attenuation (dB/m/kHz)
0.10	1470.	1.28	0.01
--	1480.	1.32	0.01

Table A2 *Geoacoustic properties for Fig. 27.*

Thickness (m)	Sound Speed (m/s)	Density (g/cc)	Attenuation (dB/m/kHz)
0.10	1470.	1.28	0.01
0.50	1480.	1.32	0.01
0.07	1470.	1.28	0.01
--	1480.	1.32	0.01

Document Data Sheet

Security Classification		Project No.
UNCLASSIFIED		04-C
Document Serial No.	**Date of Issue**	**Total Pages**
SR-344	April 2001	37 pp.

Author(s)

Holland, C.W.

Title

Shallow water coupled scattering and reflection measurements

Abstract

The characteristics of shallow water reverberation are often controlled by interaction with the seabed. This interaction includes both reflection and scattering processes. New techniques for measuring shallow water reflection and scattering have been developed that are coupled. The coupled nature of the measurements implies not only that they are conducted at the same locations, but that the measurements of the reflection provide significant keys for unravelling the scattering data. In particular, very high resolution geoacoustic data are extracted from the reflection data, which provide crucial inputs for the modelling of the scattering data. 1-6 kHz reflection and scattering measurements from the Malta Plateau illustrate the advantages of the coupled measurement approach.

Keywords

Issuing Organization

North Atlantic Treaty Organization
SACLANT Undersea Research Centre
Viale San Bartolomeo 400, 19138 La Spezia, Italy

[From N. America: SACLANTCEN (New York) APO AE 09613]

Tel: +39 0187 527 361
Fax:+39 0187 527 700

E-mail: library@saclantc.nato.int

The SACLANT Undersea Research Centre provides the Supreme Allied Commander Atlantic (SACLANT) with scientific and technical assistance under the terms of its NATO charter, which entered into force on 1 February 1963. Without prejudice to this main task - and under the policy direction of SACLANT - the Centre also renders scientific and technical assistance to the individual NATO nations.

This document is approved for public release.
Distribution is unlimited

SACLANT Undersea Research Centre
Viale San Bartolomeo 400
19138 San Bartolomeo (SP), Italy

tel: +39 0187 527 (1) or extension
fax: +39 0187 527 700

e-mail: library@saclantc.nato.int

NORTH ATLANTIC TREATY ORGANIZATION